

## Reflective Interferometric Fourier Transform Spectroscopy: A Self-Compensating Label-Free Immunosensor Using Double-Layers of Porous SiO<sub>2</sub>

Claudia Pacholski,<sup>†</sup> Christine Yu,<sup>†</sup> Gordon M. Miskelly,<sup>‡</sup> Denis Godin,<sup>§</sup> and Michael J. Sailor<sup>\*,†</sup>

*Department of Chemistry and Biochemistry, University of California, San Diego, 9500 Gilman Drive, Dept. 0358, La Jolla, California 92093-0358, Department of Chemistry, The University of Auckland, Private Bag 92019, Auckland, New Zealand, and Environment and Natural Resources, NSERC/CRSNG, 350 Albert, Ottawa, ON, K1A 1H5 Canada*

Received October 11, 2005; E-mail: msailor@ucsd.edu

Most optical transducers for label-free biosensing involve measurement of a change in the refractive index of a material induced upon analyte binding. While surface plasmon resonance (SPR) films,<sup>1,2</sup> resonant and nonresonant diffraction gratings,<sup>3,4</sup> Reflectometric Interference (RIFS) layers,<sup>5</sup> and Fabry–Pérot interferometers<sup>5</sup> show very sensitive responses to small changes in refractive index, these methods are often limited by zero point drift arising from changes in temperature, matrix composition, or nonspecific binding to the analytical surface. A double-beam interferometer (Mach–Zender-type, for example), in which one optical path acts as a reference channel, provides an excellent means of compensating for drift. Various implementations of double-beam correction have been employed in microscale biosensor systems, generally involving two spatially distinct regions of a chip.<sup>3,6</sup> Because the sample and reference channels are separated in the *X–Y* plane, such designs pose significant alignment and manufacturability challenges, especially upon incorporation into high-throughput arrays. We have recently described a self-compensating interferometric biosensor comprised of two layers of porous SiO<sub>2</sub>, stacked one on top of the other.<sup>7</sup> The reflectivity spectrum displays a complex interference pattern that arises from a combination of Fabry–Pérot interference from these layers, and it was found that compensation for drift caused by changes in the sample matrix can be achieved by appropriate analysis of the Fourier transform of the spectrum. The method, referred to as Reflective Interferometric Fourier Transform Spectroscopy, or RIFTS, was demonstrated in a test case using nonspecifically bound bovine serum albumin (BSA).

In this work, the first example of specific sensing using RIFTS is demonstrated, using a protein A capture probe and a rabbit immunoglobulin G target analyte. The amplitudes of the peaks in the fast Fourier transform of the interference spectrum depend on the refractive index contrast at the interfaces of the double-layer. The ratio of the amplitudes of the two main peaks (corresponding to layers 2 and 3 in Figure 1) provides a sensitive means to detect analyte binding at the solution/film interface and significantly reduces the effect of fluctuations in lamp intensity and other experimental variables that lead to noise or baseline drift. It is found that the method is also insensitive to large changes in matrix composition caused by introduction of 100-fold excess of interferents, such as sucrose or bovine serum albumin. The method provides a robust means of determining equilibrium biomolecular binding constants.

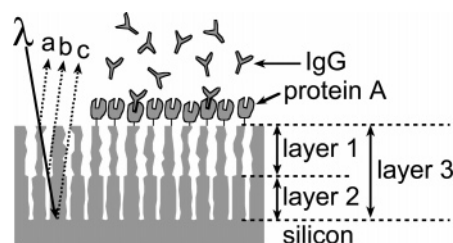


**Figure 1.** Schematic of the double-layer biosensor showing the optical paths that provide the self-correcting function to the structure. Protein A is immobilized on the top of layer 1. The three different interfering light paths are shown. Interference of beams a and b occurs from reflections at the interfaces bordering layer 1, interference of beams b and c originates from layer 2, and interference of beams a and c originates from layer 3. Binding of IgG to protein A affects the spectral interference patterns corresponding to layers 1 and 3 only. Interference arising from layer 2 is only affected by nonspecific changes in the experiment and so can be used to null the effects of zero point drift on layers 1 and 3.

A schematic diagram of the double-layer biosensor used in this work is shown in Figure 1. The structure is prepared by electrochemically etching single-crystal silicon (p-type, ca. 1 mΩcm, (100) orientation) in aqueous ethanolic HF solution (3:1 v/v 48% aqueous HF:ethanol), using a short period of high applied current (250 mA/cm<sup>2</sup> for 23 s) followed by a longer period at low current (83 mA/cm<sup>2</sup> for 115 s). The current waveform produces a high porosity, low refractive index layer on top of a lower porosity, higher refractive index layer.<sup>7</sup>

The porous Si sample is thermally oxidized (600 °C for 1 h in air) in order to stabilize the film against dissolution in aqueous media.<sup>8,9</sup> Oxidation also increases the hydrophilicity of porous Si, allowing water to effectively infiltrate the pores. The pores in both layers are large enough to admit the buffer ions and small biomolecules in the analyte matrix, but they are too small (<10 nm) to admit larger biomolecules, such as protein A or IgG. The capture probe (protein A in this study) is then adsorbed onto the top of the oxidized porous silicon structure. The position of the capture probe on the top of the film is the same as that in an SPR or RIFS device,<sup>10,11</sup> but the optical path in RIFTS passes through the solution, the protein layer, and the two underlying porous layers. In the present experiments, no specific surface attachment chemistry was employed; the protein A adheres by adsorption.

The reflectivity spectrum (Figure 2) of a double-layer film obtained at normal incidence displays a complex pattern arising from interference in all three layers represented in Figure 1. The spectrum is adequately modeled with a simple double-layer interference relationship, after the treatment of McLeod.<sup>7,12</sup> The

<sup>†</sup> University of California, San Diego.

<sup>‡</sup> The University of Auckland.

<sup>§</sup> NSERC/CRSNG.

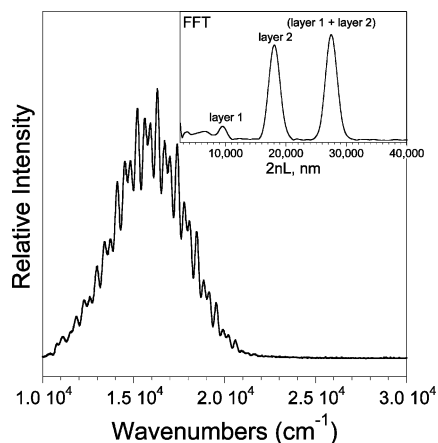


**Figure 2.** Reflectivity spectrum of a thermally oxidized porous Si double-layer biosensor film and its corresponding Fourier transform (inset). Peaks in the FFT labeled “layer 1”, “layer 2”, and “layer 1 + layer 2” (equivalent to “layer 3”) are assigned as depicted in Figure 1. Sample contains the capture probe protein A on the top of layer 1. Spectrum is measured in aqueous PBS solution and is not corrected for instrumental spectral response.

reflectance  $R$  of light from a double-layer stack consisting of two layers of differing refractive indices is given by (eq 1)

$$R = (\rho_a^2 + \rho_b^2 + \rho_c^2) + 2\rho_a\rho_b\cos(2\delta_1) + 2\rho_b\rho_c\cos(2\delta_2) + 2\rho_a\rho_c\cos[2(\delta_1 + \delta_2)] \quad (1)$$

where  $\delta_i$  represents the phase relationship<sup>7</sup> of layer  $i$  given by (eq 2):

$$\delta_i = \frac{2\pi n_i L_i}{\lambda} \quad (2)$$

where  $n_i$  represents the refractive index of layer  $i$  with thickness  $L_i$ . The terms  $\rho_a$ ,  $\rho_b$ , and  $\rho_c$  represent the index contrast at each of the reflective interfaces  $a$ ,  $b$ , or  $c$  (Figure 1):

$$\rho_a = \frac{n_{\text{soln}} - n_1}{n_{\text{soln}} + n_1}, \rho_b = \frac{n_1 - n_2}{n_1 + n_2}, \rho_c = \frac{n_2 - n_{\text{Si}}}{n_2 + n_{\text{Si}}} \quad (3)$$

The terms  $n_{\text{soln}}$ ,  $n_1$ ,  $n_2$ , and  $n_{\text{Si}}$  represent the refractive index of the aqueous layer, layer 1, layer 2, and bulk Si, respectively. The quantities  $n_1$  and  $n_2$  represent the average index of the porous layer and everything it contains (silicon,  $\text{SiO}_2$ , solution, etc.). The quantity  $n_{\text{soln}}$  represents the index at the near-surface region of layer 1; this corresponds to the region including the immobilized protein A capture probe (Figure 1).

The basic principle behind the use of the Fourier transform to extract the relevant optical parameters has been published.<sup>7</sup> The Fourier transform of the reflectivity spectrum has three main components, as shown in the inset to Figure 2. The amplitude of each FFT peak is related to the amplitude of each cosine term in eq 1 by eq 4:

$$A_1 = k\rho_a\rho_b, A_2 = k\rho_b\rho_c, A_3 = k\rho_a\rho_c \quad (4)$$

where  $A_1$ ,  $A_2$ , and  $A_3$  are the amplitudes of the FFT peaks corresponding to layers 1, 2, and 3 of Figure 1, respectively, and  $k$  is a proportionality constant that accounts for the fact that the spectrum is not corrected for instrumental response. When the refractive index of these layers changes (such as occurs with a nonspecific change in solution composition), or if there are fluctuations in lamp intensity, the magnitude of  $A_i$  for layers 1, 2, and 3 can change since they share common interfaces. However,

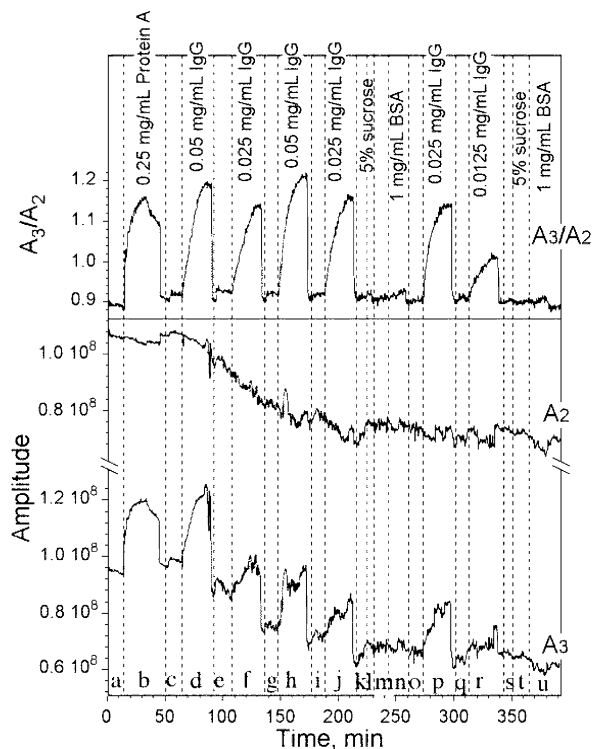


**Figure 3.** Effect of addition of rabbit IgG, sucrose, and BSA on the amplitude of the FFT peaks measured from a protein A-modified double-layer sensor.  $A_2$  and  $A_3$  represent the amplitudes of the FFT peaks corresponding to layer 2 and layer 3, respectively. The ratio of  $A_3/A_2$  eliminates baseline drift and significantly reduces noise in the measurement of rabbit IgG binding: (a) PBS buffer; (b) 0.25 mg/mL of protein A in PBS, followed by PBS, then 0.1 M acetic acid; (c) PBS; (d) 0.05 mg/mL of rabbit IgG, followed by PBS, then 0.1 M acetic acid; (e) PBS; (f) 0.025 mg/mL of rabbit IgG, followed by PBS, then 0.1 M acetic acid; (g) PBS; (h) 0.05 mg/mL of rabbit IgG, followed by PBS, then 0.1 M acetic acid; (i) PBS; (j) 0.025 mg/mL of rabbit IgG, followed by PBS, then 0.1 M acetic acid; (k) PBS; (l) 50 mg/mL of sucrose in PBS; (m) PBS; (n) 1 mg/mL of BSA in PBS, followed by PBS, then 0.1 M acetic acid; (o) PBS; (p) 0.025 mg/mL of rabbit IgG, followed by PBS, then 0.1 M acetic acid; (q) PBS; (r) 0.0125 mg/mL of rabbit IgG, followed by PBS, then 0.1 M acetic acid; (s) PBS; (t) 50 mg/mL of sucrose in PBS, followed by PBS; (u) 1 mg/mL of BSA in PBS, followed by PBS, then 0.1 M acetic acid and PBS.

when specific binding occurs at the capture probes immobilized at the top interface of layer 1 (Figure 1), only the magnitudes of  $A_1$  and  $A_3$  are expected to change. Thus, a ratio of either  $A_1$  or  $A_3$  to  $A_2$  is predicted to compensate for changes that are not derived from binding to the capture probe. For example, the quantity  $A_3/A_2$  is related to the index contrast at two of the three interfaces present in the double-layer (eq 4) by eq 5:

$$\frac{A_3}{A_2} = \frac{k\rho_a\rho_c}{k\rho_b\rho_c} = \frac{\rho_a}{\rho_b} \quad (5)$$

All three of the quantities  $A_1$ ,  $A_2$ , and  $A_3$  contain information that can be used to compensate for zero point drift. However, the peaks associated with layers 2 and 3 are typically much larger than for layer 1 (Figure 2) since the porous silicon–silicon interface has a much higher index contrast than the other two interfaces. The amplitudes  $A_2$  and  $A_3$ , and the ratio  $A_3/A_2$  are presented in Figure 3, showing the ability of this ratio to correct for zero point drift.

The significant baseline drift observed in the plots of  $A_2$  and  $A_3$  versus time is ascribed to instrumental drift, scattering in the light path, or degradation of the porous silicon structure.<sup>8</sup> The noise corresponds to lamp intensity fluctuations, changing cell temper-

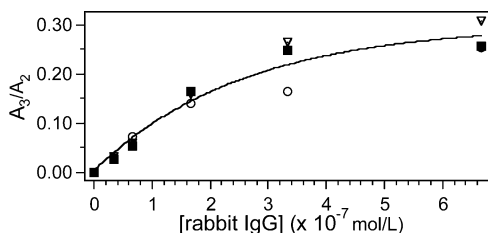


**Figure 4.** Binding curve used to determine the equilibrium dissociation constant for the binding of rabbit IgG to a protein A-modified porous silicon surface using RIFTS. The plot shows the dependence of the ratio between the amplitudes of FFT peak 3 and FFT peak 2 ( $A_3/A_2$ ) on concentration of rabbit IgG in the analyte solution. Data for three trials on three separate chips are shown (circles, triangles, squares). Solid trace represents a fit to a Langmuir isotherm, yielding an equilibrium dissociation constant  $K_D$  of  $3 \times 10^{-7}$  M.

ature, bubbles in the flow cell, and other undetermined experimental variables. Both the baseline drift and the noise in the plots of  $A_2$  and  $A_3$  are correlated, and they are effectively eliminated in the ratio of  $A_2$  to  $A_3$ , as shown in Figure 3. This leaves the interaction of protein A and rabbit IgG as the major determinant of the sensor response. Biomolecules that do not interact with protein A (such as BSA) cause little change in the amplitudes (Figure 3 regions n and u), indicating that there are minimal nonspecific interactions with the surface. Smaller molecules, such as sucrose and buffer, penetrate all the layers of the structure, but do not interact specifically with protein A and also exert minimal influence on the quantities  $A_1$ ,  $A_2$ , or  $A_3$ . The large response to protein A (Figure 3, region b) suggests that exposure to high concentrations of protein A (0.25 mg/mL) leads to either a closely packed or multilayer adsorption, with the number of adsorbed protein A molecules being greatly reduced upon rinsing with buffers and 0.1 M acetic acid (end of region b). This type of behavior has been reported previously for the adsorption of protein A onto gold colloids.<sup>13</sup>

The response of the protein A-modified sensor to IgG (ratio change ca. 0.27 for 0.05 mg/mL) is approximately 10 times greater than the change observed for strongly adsorbed protein A (ca. 0.029). Part of this difference is due to the differences in molecular weight (protein A = 42 kDa, rabbit IgG = ca. 150 kDa), which can account for ~3.6-fold difference in response. The additional difference may be due to protein A binding two IgG molecules under these conditions, as has been reported for some solution studies,<sup>14</sup> or to differences in the refractive index of IgG relative to protein A. It should also be noted that the sensor response here

is proportional to a change in the interfacial refractive index *contrast* rather than just a change in magnitude of the index.

The RIFTS biosensor provides a quantitative measure of equilibrium binding constants. The thermodynamic equilibrium binding constant can be obtained from the  $A_3/A_2$  signal at equilibrium for various analyte concentrations by application of a Langmuir fit to the binding isotherm (Figure 4 and Supporting Information).<sup>15,16</sup> A fit of the average values of three trials yields an equilibrium dissociation constant  $K_D$  of  $3 \times 10^{-7}$  mol/L for rabbit IgG/protein A, consistent with the published values.<sup>17–19</sup>

**Acknowledgment.** This project has been funded in part with Federal funds from the National Science Foundation (Grant No. DMR-0503006) and the Air Force Office of Scientific Research (Grant No. F49620-02-1-0288). M.J.S. is a member of the Moores UCSD Cancer Center and the UCSD NanoTUMOR Center under which this research was conducted and partially supported by NIH Grant U54 CA 119335. C.P. thanks the Deutsche Forschungsgemeinschaft (PA 925/1-1) for a postdoctoral fellowship.

**Supporting Information Available:** Experimental procedures, details of the Langmuir isotherm fit. This material is available free of charge via the Internet at <http://pubs.acs.org>.

## References

- (1) Homola, J.; Yee, S. S.; Gauglitz, G. *Sens. Actuators, B* **1999**, *54*, 3–15.
- (2) Nikitin, P. I.; Beloglazov, A. A.; Kochregin, V. E.; Valeiko, M. V.; Ksenevich, T. I. *Sens. Actuators, B* **1999**, *54*, 43–50.
- (3) Yu, F.; Knoll, W. *Anal. Chem.* **2004**, *76*, 1971–1975.
- (4) Bailey, R. C.; Hupp, J. T. *Anal. Chem.* **2003**, *75*, 2392–2398.
- (5) Brecht, A.; Gauglitz, G. *EXS* **1997**, *81* (Frontiers in Biosensorics II), 1–16.
- (6) Boozer, C.; Yu, Q. M.; Chen, S. F.; Lee, C. Y.; Homola, J.; Yee, S. S.; Jiang, S. Y. *Sens. Actuators, B: Chem.* **2003**, *90*, 22–30.
- (7) Pacholski, C.; Sartor, M.; Sailor, M. J.; Cunin, F.; Miskelly, G. M. *J. Am. Chem. Soc.* **2005**, *127*, 11636–11645.
- (8) Lees, I. N.; Lin, H.; Canaria, C. A.; Gurtner, C.; Sailor, M. J.; Miskelly, G. M. *Langmuir* **2003**, *19*, 9812–9817.
- (9) Gao, T.; Gao, J.; Sailor, M. J. *Langmuir* **2002**, *18*, 9953–9957.
- (10) Gauglitz, G. *Anal. Bioanal. Chem.* **2005**, *381*, 141–155.
- (11) Hanel, C.; Gauglitz, G. *Anal. Bioanal. Chem.* **2002**, *372*, 91–100.
- (12) McLeod, H. A. *Thin-Film Optical Filters*; Adam Hilger, Ltd.: Bristol, 1986.
- (13) Horisberger, M.; Clerc, M.-F. *Histochemistry* **1985**, *82*, 219–223.
- (14) Yang, L.; Biswas, M. E.; Chen, P. *Biophys. J.* **2003**, *84*, 509–522.
- (15) Schuck, P. *Annu. Rev. Biophys. Biomol. Struct.* **1997**, *26*, 541–566.
- (16) Saha, K.; Bender, F.; Gizeli, E. *Anal. Chem.* **2003**, *75*, 835–842.
- (17) Jonsson, S.; Kronvall, G. *Eur. J. Immunol.* **1974**, *4*, 29–33.
- (18) Lindmark, R.; Biriell, C.; Sjoquist, J. *Scand. J. Immunol.* **1981**, *14*, 409–420.
- (19) Lancet, D.; Isenman, D.; Sjoedahl, J.; Sjoquist, J.; Pecht, I. *Biochem. Biophys. Res. Commun.* **1978**, *85*, 608–614.

JA056702B